ATTACHMENT A

STRUCTURAL ANALYSIS

OF

WORN SURVEILLANCE SPECIMEN HOLDER TUBES

SC-269

Rec'd w/ltr dtd

4-13-76

For a preliminary look at the SHT in a damaged condition, we may use the approach given by Gorman (1). We treat the damaged section as a beam simply supported at each end and assume the damage is located in the center. If we take a worst case approach to the damage, we can approximate it as shown:

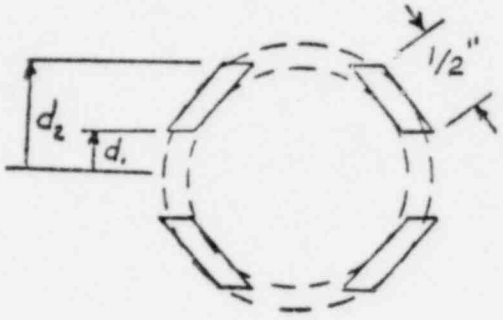

$d_2 = 1.372$ "

$d_1 = 1.018$ "

We consider the damage to be severe enough to leave only four ligaments with a width of 1/2 inch, a thickness of .120 inch and a length of 1/2 inch.

The moment of inertia of this reduced section is then given by:

$$I = 4 \int_{a_1}^{\quad} t\, x^2\, dx = .3457 \text{ inches}^4$$

where t is the wall thickness = .120 inch. The cross sectional area of the remaining ligaments is then:

$$A = 4 \times t \times 1/2" = .24 \text{ inches}^2.$$

Treating the damaged beam as being symmetric about the discontinuous section, the first natural frequency is given as

$$f_1 = \frac{(2\beta_1)^2}{2\pi(L)^2} \sqrt{\frac{E_1 I_1}{\rho_1 A_1}}$$

where β_1 is a constant dependent upon the reduced bending rigidity and the mass per unit length. Using these constants

---

(1) Gorman, D. I., Free Vibration Analysis of Beams and Shafts, John Wiley and Sons, N.Y., N.Y., 1975.

$$\alpha = \left(\frac{E_2 I_2}{E_1 I_1}\right)^{1/4} = .67 \qquad \text{and} \qquad \phi = \left(\frac{\rho_2 A_2}{\rho_1 A_1}\right)^{1/4} = .66$$

and $\mu = 1-\gamma = .993$ where γ is the normalized length of the damage, we can choose β_1 from a linear interpolation of the tables listed in Gorman. The subscript 1 refers to the undamaged section and 2, the damaged section. We choose β_1 to be 1.5628 (which should be accurate to a few percent) based on an overall beam length of 68 inches. We can now predict the ratio of the first natural frequencies as

$$\frac{f_1(\text{damaged})}{f_1(\text{good})} = \frac{(2\beta_1(\text{damaged})^2}{(2\beta_1(\text{good})^2} \quad \frac{2\pi L_1^2}{2\pi L_1^2} \sqrt{\frac{E_1 I_1}{\rho_1 A_1}} \Big/ \sqrt{\frac{E_1 I_1}{\rho_1 A_1}}$$

$$= \left(\frac{\beta_1(\text{damaged})}{\beta_1(\text{good})}\right)^2$$

$$= \left(\frac{1.5628}{1.5708}\right)^2 = .9898$$

This is approximately a 1% difference in natural frequencies.

The change in amplitude can be found from the solution of the system of equations resulting from the matching of the boundary conditions at the interface of the discontinuity. The amplitude at midspan is now given as

$$r = B_2 \cos \phi + D_2 \cosh \phi$$

$$= B_2 + D_2$$

$$= 3.073 - 2.017 = 1.056$$

Forming the ratio between this value at that of the undamaged beam we have

$$\frac{r(\text{damaged})}{r(\text{good})} = \frac{1.056}{1} = 1.056$$

This represents an approximate amplitude increase of 5.6%.

Additionally we can simply calculate a stress ratio due to bending.

$$\frac{\sigma(\text{damaged})}{\sigma(\text{good})} = \frac{\frac{MC}{I}(\quad)}{\frac{MC}{I}(\quad)}$$

For a moment that remains constant (nearly the case if the damage length is small), this reduces to

$$\frac{\sigma(\text{damaged})}{\sigma(\text{good})} = \frac{I(\text{good})}{I(\text{damaged})} \cdot \frac{C(\text{damaged})}{C(\text{good})}$$

The moment of inertia of a good tube is

$$I = \frac{\pi(D_o^4 - D_i^4)}{64}$$

D_o = outside diameter = 3.5 inch

D_i = inside diameter = 3.5 - .24 inch

$I = 1.822$

Therefore, the bending stresses will rise by a factor of

$$\frac{\sigma(\text{damaged})}{\sigma(\text{good})} = \frac{1.822}{.3457} \cdot \frac{1.372}{1.75} = 4.13.$$

From Topical Report 10,039 the measured stress in this area was found to be 300 psi. In the damaged section we would expect the stress to now rise to 1239 psi. The safety factor becomes, for the case of severe damage,

$$SF = \frac{13500}{1239} = 10.9$$

This is in addition to any safety factor built in to the allowable stress level.

The Euler buckling load is given as

$$P_{cr} = n\pi^2 EA/(L/r)^2$$

where r = least radius of gyration

and $I = Ar^2$ or $r = \sqrt{\frac{I}{A}}$

Therefore, r for the damaged tube = $\sqrt{\frac{.3457}{.24}}$ = 1.2

and L/R = 86.67.

Now $P_{cr} = n\pi^2\ 26 \times 10^2 \times .24/(86.67)^2$

P_{cr} = 8199 lbs

In this case n = 1 (pinned-pinned ends) which is the worst case. This buckling load is much greater than the applied preload even if we assume a large effect due to differential thermal expansion.

The actual natural frequencies to be expected can be calculated, again using Gorman. The first natural frequency of the lower (ogee) section can be approximated by

$$f_1 = \frac{(\beta_1)^2}{2\pi L^2}\sqrt{\frac{EIg}{w}}$$

E = Young's Modulus = 26×10^6 psi

$$I = \frac{\pi(D_o^4 - D_i^4)}{64} = 1.822$$

g = 386 in/sec^2

L = 68 in

β_1 = 3.927

$w = w_{steel} + w_{water} + w_{virtual}$ lb/in

$$w_s = \rho_s \frac{\pi}{4}(D_o^2 - D_i^2) = .3606 \text{ lb/in}$$

$$w_{water} = \rho_{water} \frac{\pi D_i^2}{\pi} = .2174 \text{ lb/in}$$

$$w_{virtual} = \rho_{water} \frac{\pi D_o^2}{4} = .2506 \text{ lb/in}$$

$$f_1 = \frac{(3.927)^2}{2\pi(68)^2} \sqrt{\frac{26 \times 10^6 \times 1.822 \times 386}{.8289}} = 78.84 \text{ hertz}$$

Accounting for the damaged section we have

$$f_{1 \text{ damaged}} = 78.84 \times .9898 = 78.04 \text{ hertz}$$

For the upper section we have

$$L = 100 \text{ in}$$

$$w_{steel} = .3073 \text{ lb/in}$$

$$w_{water} = .1558 \text{ lb/in}$$

$$w_{virtual} = \rho_{water} \frac{\pi d_o^2}{4} \frac{b^2+a^2}{b^2-a^2} = 2.2198$$

$$I = \frac{\pi(D_o^4 - D_i^4)}{64} = 1.1276$$

$$f_1 = \frac{(3.927)^2}{2\pi(100)^2} \sqrt{\frac{26 \times 10^6 \times 1.1276 \times 386}{2.6829}} = 15.94 \text{ hertz}$$

Even with the heavy damage previously assumed, this frequency will remain virtually unchanged. The difference in predicted natural frequencies (a factor of 5) also tends to substantiate the choice for β_1 of 3.927 which is the value used for clamped-simply supported end conditions.

The analysis of the wear mechanism is extremely difficult. On the surface we can say that the spacer disks wore through the SHT. This is obvious and therefore the pushrods with disks must be removed. The excitation mechanism or forcing function is not so readily explained. One possibility is explored below.

Consider the following model for the pushrod assembly:

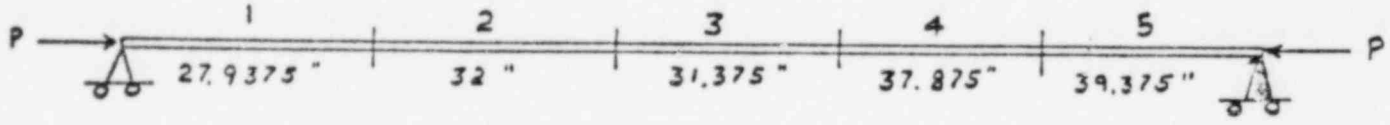

Rod $D = .5$ inch

$I = \frac{\pi D^4}{64} = .003068 \text{ in}^4$

$E = 26 \times 10^6$ psi

$g = 386 \text{ in/sec}^2$

$\rho_{steel} = .283 \text{ lb/in}^3$

$\rho_{water} = 45 \text{ lb/ft}^3$

$w_{steel} = .0556 \text{ lb/in}$

$w_{virtual} = .0051 \text{ lb/in}$

$w_{total} = .0607 \text{ lb/in}$

$$f_1 = \frac{\pi}{2L^2}\sqrt{\frac{EIg}{w}}\sqrt{1 - \frac{P}{P_{cr}}} \quad (2) \quad \text{(simple-simple supports)}$$

where P_{cr} = Euler buckling load

$= \frac{\pi^2 EI}{L^2}$ (1st mode, simple-simple ends)

and the effect of the spacers is neglected.

Depending on what spacers are against the tube wall at a

---

(2) Timoshenko, S., Young, D. H., Weaver, W., Jr., Vibration Problems in Engineering, John Wiley and Sons, N.Y., N.Y., 1974.

given time, the natural frequencies can vary tremendously. This, coupled with the variable preload and the pre-bent (installed) condition make any natural frequency calculations subject to large errors. However, for a quick analysis we construct the following table:

Span	f_1 (P=0(Hz)	f_1 (P=200 lbs)(Hz)	P_{cr} (lbs)
1	45.3	40.6	1009
2	34.6	29.7	769
3	35.9	31.1	800
4	24.7	19.7	549
5	22.8	17.8	509
1+2	9.85	2.91	219
2+3	8.81	0	196
3+4	7.38	0	164
4+5	5.93	0	132
1+2+3	4.24	0	94
2+3+4	3.45	0	77
3+4+5	3.00	0	67
1+2+3+4	2.12	0	47
2+3+4+5	1.79	0	40
1+2+3+4+5	1.25	0	28

The mechanisms which may excite these various modes are summarized in the following tables.

Thermal shield radial deflection peaks

Hz	SHT Span number with nearby resonant frequencies	
	P=0	P=200
9.5	1+2,2+3	---
12	---	---
15	---	---
17.5	---	5
20	---	4
23	5,4	---
29	---	2
31	---	3
37.5	3	1

As we have seen, the natural frequencies vary with the end load and spacer contact. Although the frequency predictions of the pushrod are certainly not precise, it does seem apparent that they are of a low order of magnitude and at least in the region of possible forcing mechanisms. The radial displacements of the thermal shield are quite small (only on the order of several mils peak to peak) and with the reasonably well damped system expected inside the SHT, the aligning of the pushrod natural frequencies with external forcing functions may not be sufficient to cause excessive wear.

However, there is a small leakage path through the SHT to the upper head region. The expected pressure drop from inlet to outlet conditions, it is felt, is sufficient to cause a localized velocity between the spacer disk and SHT wall of somewhere in the neighborhood of 20-30 feet per second. This flow over the spacer disk should be sufficient to cause vortices to be shed with frequencies of at least several hundred hertz. This could cause the spacer disk to vibrate with very small amplitudes. These potential "grinders" may now be moved around the inside of the SHT by some as yet undefined coupling between the thermal shield motions and the overall pushrod. There may be a hydroelastic coupling between the SHT walls and the pushrod or perhaps the specimen capsule itself transmits the SHT support motions to the pushrod. It does seem likely, however, that the coupled problem of vortex shedding from the disks and overall pushrod motions caused the excessive wear.

ATTACHMENT B

ADDITIONAL DETAILED RESULTS

FROM

OCONEE 1 HFT

INTERNALS VIBRATION MEASUREMENTS

3.4 RESULTS AND DISCUSSION FROM THERMAL SHIELD MEASUREMENTS

3.4.1 Thermal Shield Accelerometers

3.4.1.1 Location of Thermal Shield Accelerometers. Six biaxial accelerometers were installed around the periphery of the thermal shield. Three of the six accelerometers were located in the W-X quadrant. These accelerometers were denoted as TS2, TS3, and TS4. Each of the other three quadrants contained one accelerometer. The X-Y quadrant contained accelerometer TS5, the Y-Z quadrant contained accelerometer TS6, and the Z-W quadrant contained accelerometer TS1. The radial direction for each axis was denoted with an R, and the tangential axis was denoted as a T. These accelerometers performed satisfactorily throughout the entire test program, except for TS2R and TS2T which failed during the first few days of the hot functional test program. Appendix F shows the location of each of the accelerometer axes. The installation and a further detailed description of these transducers is contained in Volume I.

3.4.1.2 Results from the Thermal Shield Accelerometers. Figure 3.4.1 shows the acceleration amplitude for each thermal shield accelerometer axis for four-pump and no-pump operation at 530°F. This figure shows the amplitude of the radial accelerometers at four pumps exceeds the amplitude at no pump by more than 20 times. The crest factor for each of these accelerometer axes varies between 2 and 3, which indicates the signal contained no large transients. This figure also shows that the radial acceleration of the thermal shield is at least twice as much as the tangential acceleration.

Figures 3.4.3a through 3.4.3d show spectra response of accelerometer TS1R for four different pump conditions at 530°F. TS1R was chosen as representative of the spectra response from the four other radial accelerometers. These figures show that the thermal shield responds at many frequencies in the 10 to 50 Hz range. In general, the frequency content for each pump operating condition is similar, as shown in Figure 3.4.3 and Table 3.4.1.

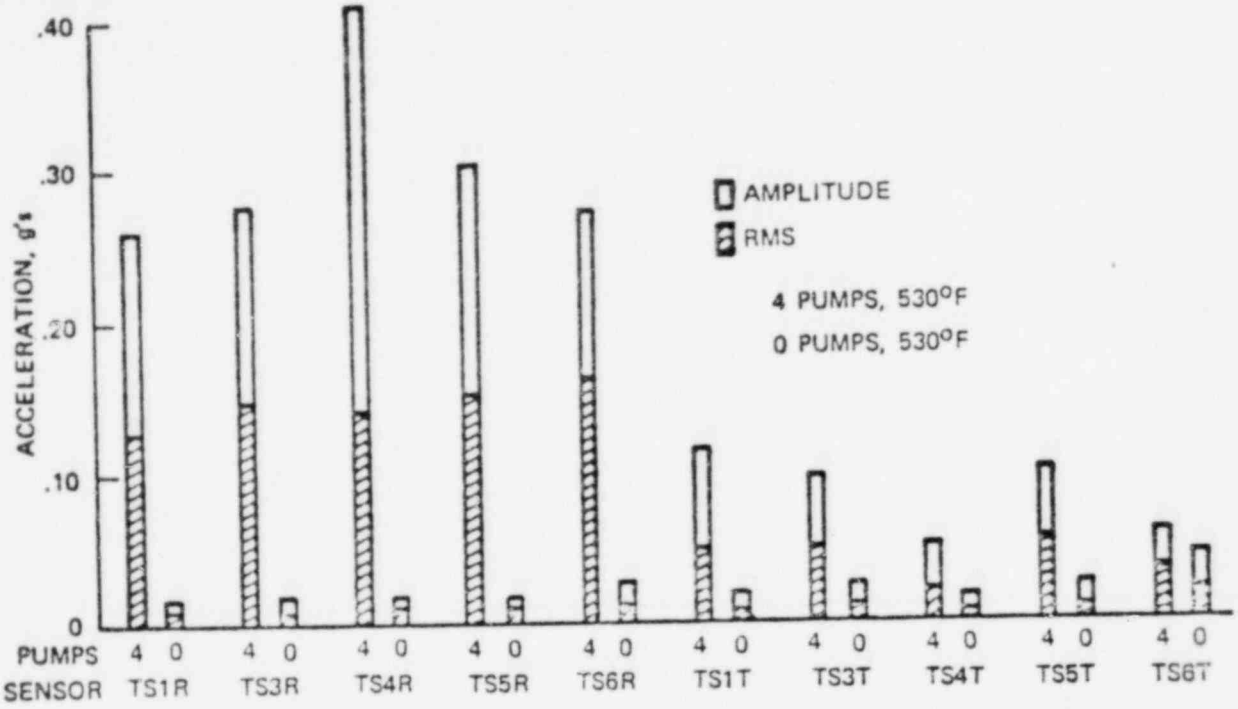

FIGURE 3.4.1 THERMAL SHIELD ACCELERATIONS, RMS AND AMPLITUDE

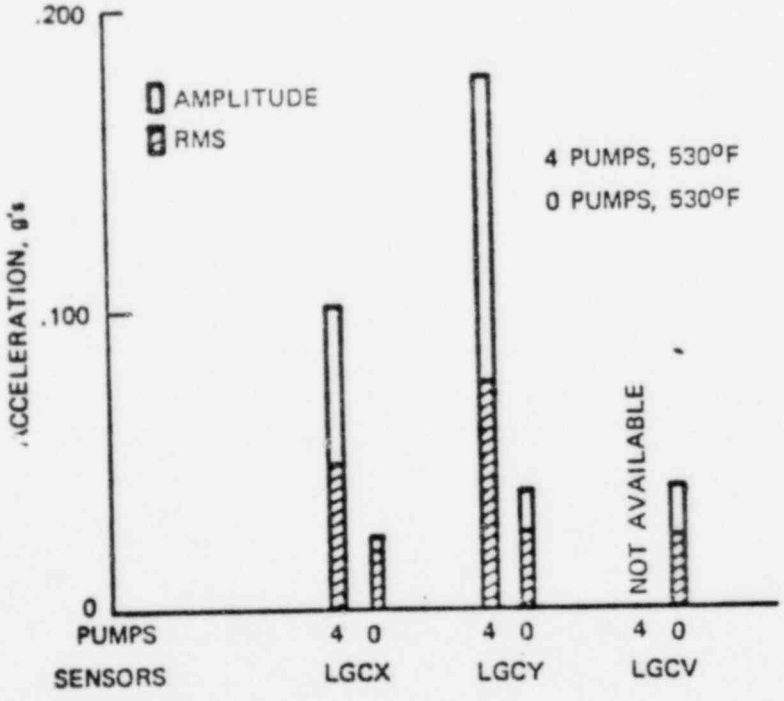

FIGURE 3.4.2 LOWER GRID ACCELERATIONS, RMS AND AMPLITUDE

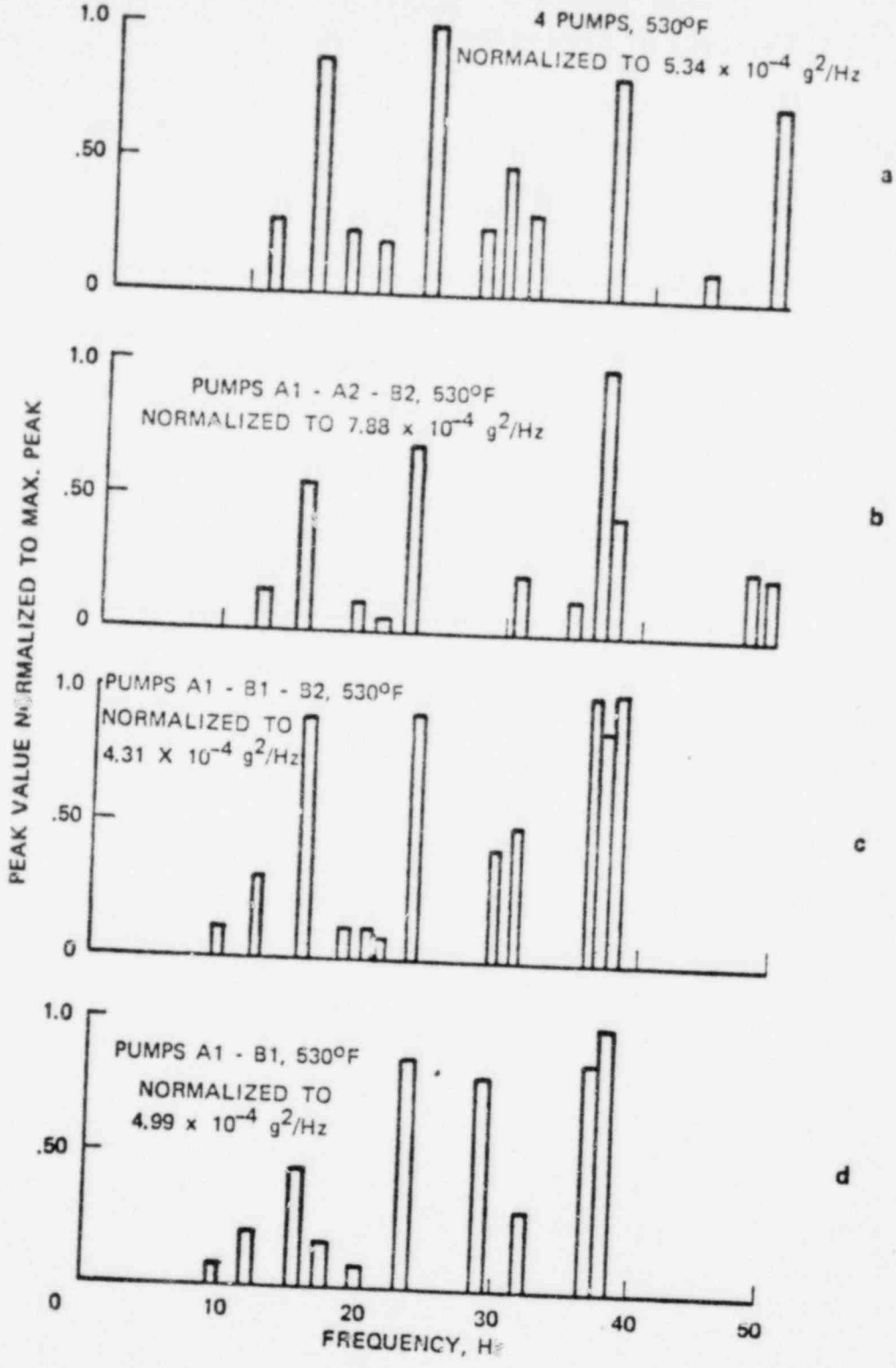

FIGURE 3.4.3 TS1R ACCELERATIONS FREQUENCY CONTENT

TABLE 3.4.1. THERMAL SHIELD RADIAL ACCELERATIONS

Test Condition	Frequency	Frequency Content Peak $g^2/Hz \times 10^4$ TS1R	TS3R	TS4R	TS5R	TS6R
4 Pumps 530°F	12.0	1.51	1.82	1.40	1.80	2.39
Tape 116 Set 174	15.0	4.66	7.00	3.91	8.11	7.71
	17.5	1.30	0.20	2.33	3.85	4.68
	20.0	1.16	1.61	0.56	0.59	8.08
	23.5	5.34	11.0	6.41	12.9	15.6
	27.5	1.44	1.77	2.91	6.31	2.02
	29.0	2.60	2.41	2.91	1.56	1.84
	31.0	1.71	2.62		1.56	1.65
	37.0	4.38	11.5	6.00	12.0	9.00
	44.0	0.66		0.84	0.84	3.21
	49.0	3.90	4.40	1.75	0.46	
Pumps A1-A2-B2	12.0	1.16	1.50			
Tape 216 Set 187	15.0	4.45	5.62			
	19.5	0.93				
	20.0	0.51	0.46			
	21.0	0.40				
	23.0	5.48	15.5			
	31.0	1.78	1.93			
	35.0	1.13				
	37.0	7.88	2.25			
	38.0	3.63	13.4			
	48.0	2.05				
	49.5	1.71	4.07			
Pumps A1-B1-B2	9.5	0.32	0.44			
Tape 117 Set 181	12.0	0.96	3.22			
	15.5	3.00	8.90			
	18.5	0.37				
	20.0	0.38	0.60			
	21.0	0.25				
	23.5	0.31	15.4			
	29.5	1.34	1.61			

Table 3.4.1 Thermal Shield Radial Accelerations (Cont'd)

Test Condition	Frequency	TS1R	TS3R	TS4R	TS5R	TS6R
Pumps A1-B1-B2 (Cont'd)	31.0	2.88	1.66			
	36.5		3.32			
	37.5	0.43	2.84			
	38.5	17.7	3.38			
Pumps A1-B1	9.0	0.46	0.38			
Tape 117 Set 180	12.0	1.03	0.63			
	15.5	2.19	7.40			
	17.5	8.90				
	20.0	0.45	0.62			
	23.5	4.25	12.1			
	29.0	3.97	3.16			
	32.0	1.51	1.61			
	37.0	3.63	5.63			
	38.0	4.93	13.4			
Pumps A1-B2 530°F	9.5	0.36	0.32			
Tape 117 Set 184	12.0	2.19	3.64			
	15.0	5.14	8.04			
	17.5	0.66	0.20			
	20.0	1.33	1.07			
	23.5	5.75	12.9			
	29.0	3.97	2.68			
	31.0	2.74	1.82			
	36.5	4.38	1.98			
	38.0	5.34	17.6			
Pumps A1-A2 530°F	9.5	0.16				
Tape 117 Set 176	12.0	2.06	0.75			
	15.0	5.96	3.86			
	17.5	0.42				
	20.0	0.34	0.20			
	21.0	0.19	0.31			
	23.5	4.66	1.45			
	31.5	1.78	0.91			
	36.5	2.57	1.02			
	38.0	2.81	7.40			
	40.5	0.38	0.42			

Figure 3.4.5 shows the displacement for various frequencies in a spectrum analysis from 0 to 50 Hz. This figure shows that the primary contribution to the displacement of the internals occurs at less than 20 Hz. Table 3.4.2 not only summarizes the results for an accelerometer, TS1R, but shows the displacement results for the other radial accelerometers. This table also shows that the primary displacement of the thermal shield occurs for frequencies less than 20 Hz. It further shows that accelerometer TS3R has the greater maximum amplitude of displacement. This value is approximately 3.85 mils.

Figure 3.4.4 shows the typical spectra response for the tangential accelerometers. This figure shows the thermal shield vibrates at many frequencies in the range of 0 to 50 Hz. Table 3.4.3 compares the response of the other four operating tangential accelerometers at various frequencies. It shows that the energy is the same at many frequencies.

3.4.2 Lower Grid Accelerometer

3.4.2.1 Location of the Lower Grid Accelerometer. Three accelerometer axes denoted LGCX, LGCY, and LGCV were installed on the lower grid. These transducer axes measured the planer and the vertical motion of the lower grid. The location of this accelerometer is shown in Appendix F. Volume I further describes the location and installation.

3.4.2.2 Results from the Lower Grid Accelerometer. Figure 3.4.2 shows the acceleration of the lower grid in three orthogonal directions. This figure shows that the signal-to-noise ratio of these three accelerometer axes was approximately 5. The crest factor for accelerometers LGCX and LGCY was approximately 2.

Figures 3.4.6a, 3.4.6b, and 3.4.6c show the normalized abridged spectra for the three axes of this accelerometer. These figures show that the accelerometer response was confined to frequencies between 10 and 40 Hz. Figure 3.4.6c shows one frequency response in the range of 40 to 50 Hz on LGCV. Table 3.4.4 contains the frequency response and amplitude of response for the lower grid accelerometer axes.

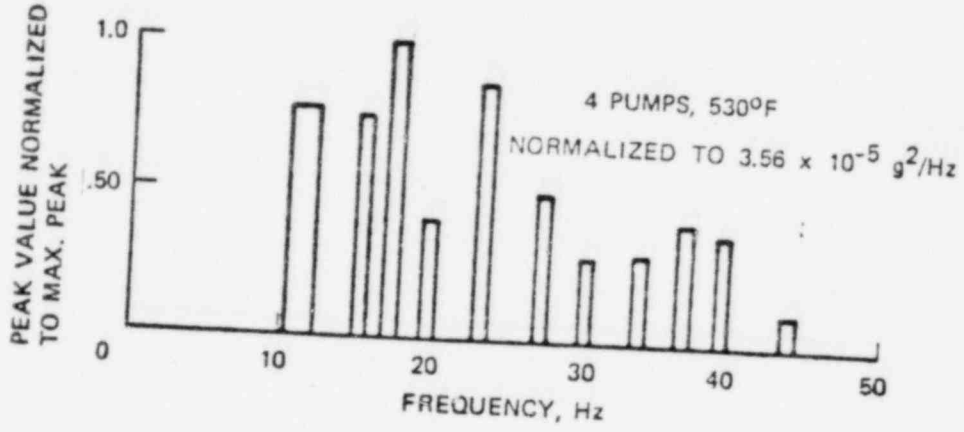

FIGURE 3.4.4 TS1T ACCELERATIONS FREQUENCY CONTENT

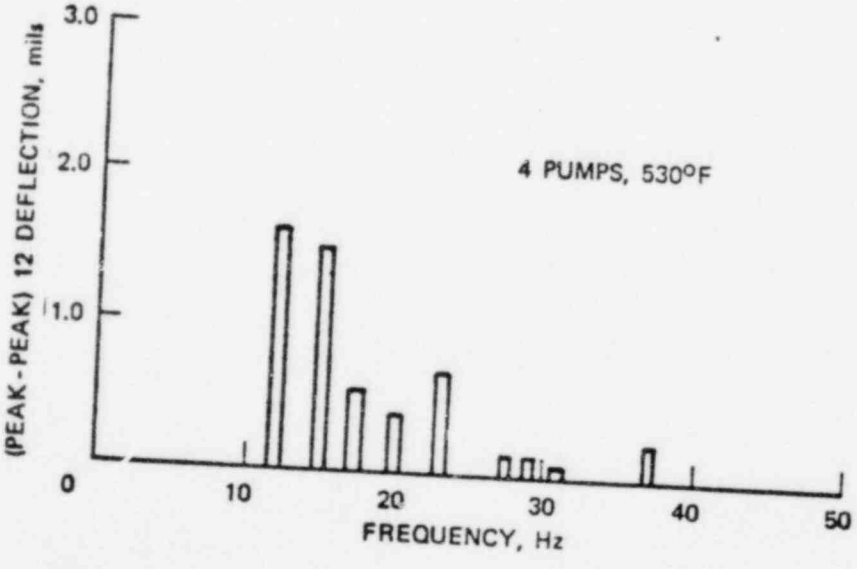

FIGURE 3.4.5 TS1R DEFLECTIONS FREQUENCY CONTENT

TABLE 3.4.2. THERMAL SHIELD RADIAL DEFLECTIONS

Sensor	Max. P-P Defl. mils	Frequency Hz	% of Total	Cum. %	P-P Defl. mils
TS1R	5.5	12	30.0	30.0	1.65
		15	27.5	57.5	1.51
		17.5	10.0	67.5	0.55
		20	7.5	75.0	0.41
		23	12.5	87.5	0.69
		27-31	7.5	95.0	0.41
		37	5.0	100.0	0.27
TS3R	7.7	12	28.6	28.6	2.20
		15.5	33.3	61.9	2.56
		17.5	0	61.9	0
		20	7.1	69.0	0.55
		23	16.7	85.7	1.28
		29	4.8	90.5	0.37
		31	4.8	95.3	0.37
		38	4.8	100.1*	0.37
TS4R	6.6	12	33.3	33.3	2.20
		15.5	25.0	58.3	1.65
		17.5	13.9	72.2	0.92
		20	0	72.2	0
		23	16.7	88.9	1.10
		29	5.6	94.5	0.37
		38	5.6	100.1*	0.37
TS5R	7.5	12	27.2	27.2	2.04
		15.5	31.8	59.0	2.38
		17.5	13.6	72.6	1.02
		20	0	72.6	0
		23	13.6	86.2	1.02
		27.5	6.8	93.0	0.51
		31	2.3	95.3	0.17
		38.5	4.5	99.8*	0.34

*Not exactly 100% due to round-off error

Table 3.4.2 Thermal Shield Radial Deflections (Cont'd)

Sensor	Max. P-P Defl. mils	Frequency Hz	% of Total	Cum. %	P-P Defl. mils
TS6R	7.0	12	31.2	31.2	2.18
		15	22.9	54.1	1.60
		17.5	14.6	68.7	1.02
		20	0	68.7	0
		23	20.8	88.8	1.46
		27-31	6.25	95.05	0.44
		37	4.17	99.22*	0.29

*Not exactly 100% due to round-off error

TABLE 3.4.3. THERMAL SHIELD TANGENTIAL ACCELERATIONS

Test Condition	Frequency	Frequency Content Peak Value $g^2/Hz \times 10^4$ TS1T	TS3T	TS4T	TS5T	TS6T
4 Pumps 530°F	11.0	0.279	0.303	0.549	0.300	0.266
Tape Set	12.0	0.279	0.276	0.250	0.323	0.328
	15.5	0.268	0.380	0.170	0.330	0.363
	17.5	0.356	1.21	0.280	0.684	0.085
	20.0	0.147	0.110	0.356	0.223	0.283
	23.5	0.308	0.132	0.333	0.258	0.213
	27.5	0.180	0.318	0.333	0.177	0.239
	29.0	--	--	--	0.235	0.275
	30.5	0.106	0.060	0.072	--	--
	33.0	--	0.076	0.106	0.088	0.101
	34.0	0.110	0.076	0.113	0.104	0.106
	36.0	--	0.238	0.144	--	0.177
	37.0	0.150	0.182	--	0.185	0.213
	39.5	0.125	0.163	0.144	0.142	0.137
	44.0	0.044	--	0.062	0.064	0.146
	49.0	--	0.125	0.038	--	0.102

3.4.5.4 Response of the Thermal Shield. Tests have been conducted to evaluate the response of the thermal shield[9]. These results have been compared to the mathematical model developed to analyze the thermal shield in the Oconee I reactor system. Results of both the test and the analysis are summarized in Table 3.4.6. As can be seen in this table, good agreement is obtained between the test and the predicted frequencies and mode shapes. However, for the second ring mode, the experiment and the analytical model did not agree. The frequencies differed by approximately 33 percent. Neither the mathematical model nor the test accounted for the effects of water surrounding the internal structures. Tests have been conducted which show that the natural frequency of a mechanical structure is altered as a result of the surrounding fluid as much as 50 percent[10]. Other effects influence the behavior of the reactor's internal structure; for example, damping. Three methods were used to determine the mode shapes that existed during operation and they are explained in Appendix C. Consistent mode shapes were found using these three methods. However, at certain frequencies, no consistent mode shapes were discernible as a result of insufficient information. Results of the modal analysis are shown in Appendix C.

The 12 Hz frequency appears to be a combination of a cantilever beam mode and a second ring mode. The cantilever beam mode is seen on the lower grid as a horizontal motion. The orientation and amplitude on the thermal shield seem to vary continuously. This randomness may be caused by the coolant flow or interaction between the lower grid and reactor vessel guide lugs.

The 15 Hz frequency appears to be a beam mode from thermal shield accelerometer information. However, the lower grid does not exhibit this frequency. This suggests that the thermal shield acts as a fixed-fixed beam, with the lower edge restrained by the thermal shield bolts.

At 20 Hz the thermal shield seems to be vibrating as a cantilever beam. The thermal shield accelerometers show no preferred orientation, but the lower grid shows a definite orientation in the Y direction. No explanation has been determined for this anomaly. The excitation results from the pump blade-passing frequency.

The 23 Hz frequency is strong on the lower grid, thermal shield, and on the bolts, but it does not seem to correspond to any expected mode shape.

For frequencies above 23 Hz only one mode shape is presently defined. This is the third ring mode at 37.5 Hz.

TABLE 3.4.6 THERMAL SHIELD NATURAL FREQUENCIES, IN AIR

Mode Shape	Calculated Frequency, Hz	Measured Frequency, Hz
n = 1 (cantilever beam)	22	--
n = 2 (second ring)	45	30.8
n = 3 (third ring)	50	49.9
n = 4 (fourth ring)	68	70.4
n = 5 (fifth ring)	96	95.3

3.5 RESULTS AND DISCUSSION OF INCORE NOZZLES AND GUIDE TUBES

3.5.1 Incore Nozzle Sensors

3.5.1.1 Location of Incore Nozzle Sensors. Two incore instrument nozzles were instrumented with four strain gages each. The nozzle 34 gages were 34N1, 34N2, 34N3, and 34N4, while nozzle 38 gages were 38N1, 38N2, 38N3, and 38N4. The strain gages were located as shown in Appendix F. All gages performed satisfactorily throughout the tests.

Four static pressure taps were installed on nozzle 33. These taps, 33P2, 33P3, and 33P4, were arranged to provide differential pressure from which the lower head flow velocity could be calculated[11]. Volume I describes the installation of the taps.

3.5.1.2 Results from Incore Nozzle Sensors. Figure 3.5.1 shows the measured stress amplitude on nozzle 34 is less than 200 psi for varying number of pumps. Results for nozzle 38 are similar. The signal-to-noise ratio varies from 1.5 to 2.6. The crest factor varies from 2 to 3.

3.6.3 Discussion of Results from Plenum Cylinder and Upper Grid Sensors

The maximum measured stress amplitude in the plenum cylinder is 160 psi. These gages were located to measure the maximum stress in the plenum cylinder. While the locations measured may not be the exact location of maximum stress, it is likely that the maximum stress in the cylinder does not approach the fatigue limit of 13,500 psi.

The upper grid and plenum cylinder sensors do not exhibit the same frequencies. This was expected since a lateral acceleration of the upper grid does not necessarily cause significant stresses in the plenum cylinder. The 23.5 Hz shown on the upper grid may be a forced vibration. The pressure variations in the external lines display a 23.5 Hz frequency, as do the thermal shield accelerometers. The pressure variations may cause the accelerations of the upper grid and/or the thermal shield. Also, it is possible that the movement of one structure is mechanically transferred to the other through the support.

3.7 SURVEILLANCE SPECIMEN HOLDER TUBE SENSORS

3.7.1 Surveillance Specimen Holder Tube Strain Gages

3.7.1.1 Location of Surveillance Specimen Holder Tube Strain Gages.

Four strain gages were attached around the circumference of the surveillance specimen holder tube. These gages, SHT1, SHT2, SHT3, and SHT4, were spaced every 90 degrees at one elevation. The location of these gages is given in Figure 1.4.1 and their installation is given in Volume I. Despite the failure of all four surveillance holder tube strain gages during the second test, reliable data at 530°F and four-pump operation were obtained, except from SHT4.

3.7.1.2 Results from Surveillance Specimen Holder Tube Strain Gages. Figure 3.7.1 shows the measured stress amplitude at 530°F for four-pump and no-pump operation. The signal-to-noise ratio varies from 1.2 to 2.0. The crest factor varies from 1.0 to 2.6. The maximum measured stress amplitude is 235 psi.

The spectral plots of data from all the strain gages show only one discernible peak at 17.5 Hz. The plot also shows wide band random stresses between 0 and 50 Hz. Figure 3.7.2 shows the power spectral density plot of SHT2 at 530°F, four-pump operation.

3.7.2 Shroud Tube Strain Gages

3.7.2.1 Location of Shroud Tube Strain Gages. Four strain gages were located around the circumference of the shroud tube. Each gage was at the same elevation and spaced every 90 degrees. These gages were designated STO1, STO2, STO3, and STO4. Figure 1.4.1 shows the location of each gage, Volume I describes the installation. All four gages performed satisfactorily throughout the hot functional test.

3.7.2.2 Results from Shroud Tube Strain Gages. Figure 3.7.3 shows the measured stresses from the shroud tube strain gages at four-pump and no-pump operation at 530°F. The signal-to-noise ratio varies from 1.2 to 2.5. The crest factor is approximately 2.6 on all four gages. The maximum measured stress amplitude is 190 psi.

Figure 3.7.4 shows the spectral plot of STO4 at 530°F and four-pump operation. After eliminating the background noise, the only discernible peak is 37.5 Hz. The balance of the plot shows random response between 0 to 50 Hz.

3.7.3 Discussion of Results from Surveillance Specimen Holder Tube Sensors

The maximum measured stress amplitude on the surveillance specimen holder tube is 235 psi and 190 psi on the shroud tube. For both structures, this is

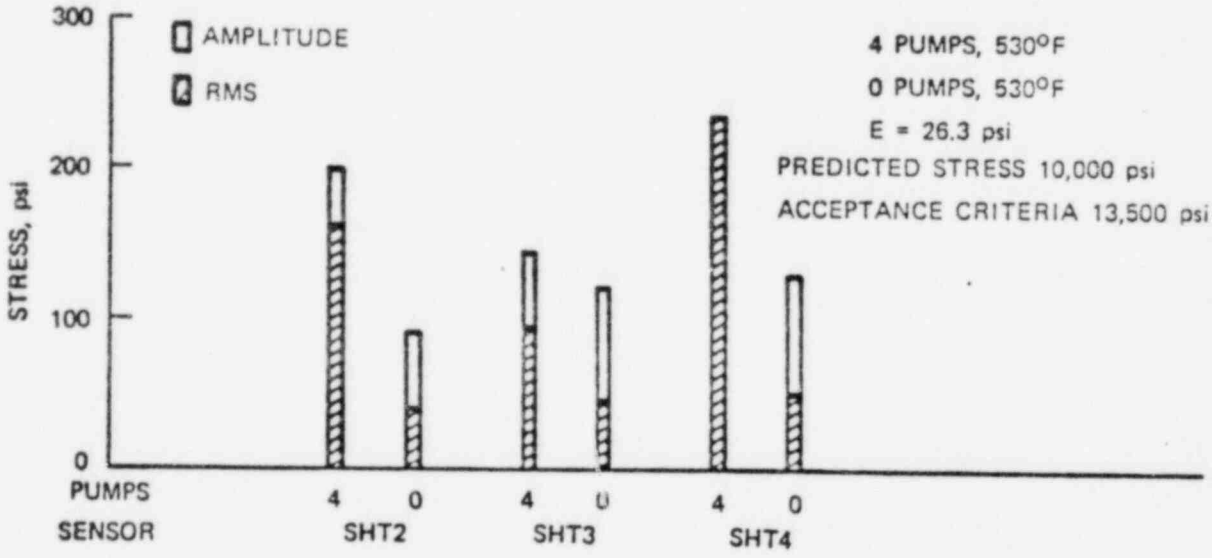

FIGURE 3.7.1 SURVEILLANCE SPECIMEN HOLDER TUBE STRESSES, RMS AND AMPLITUDE

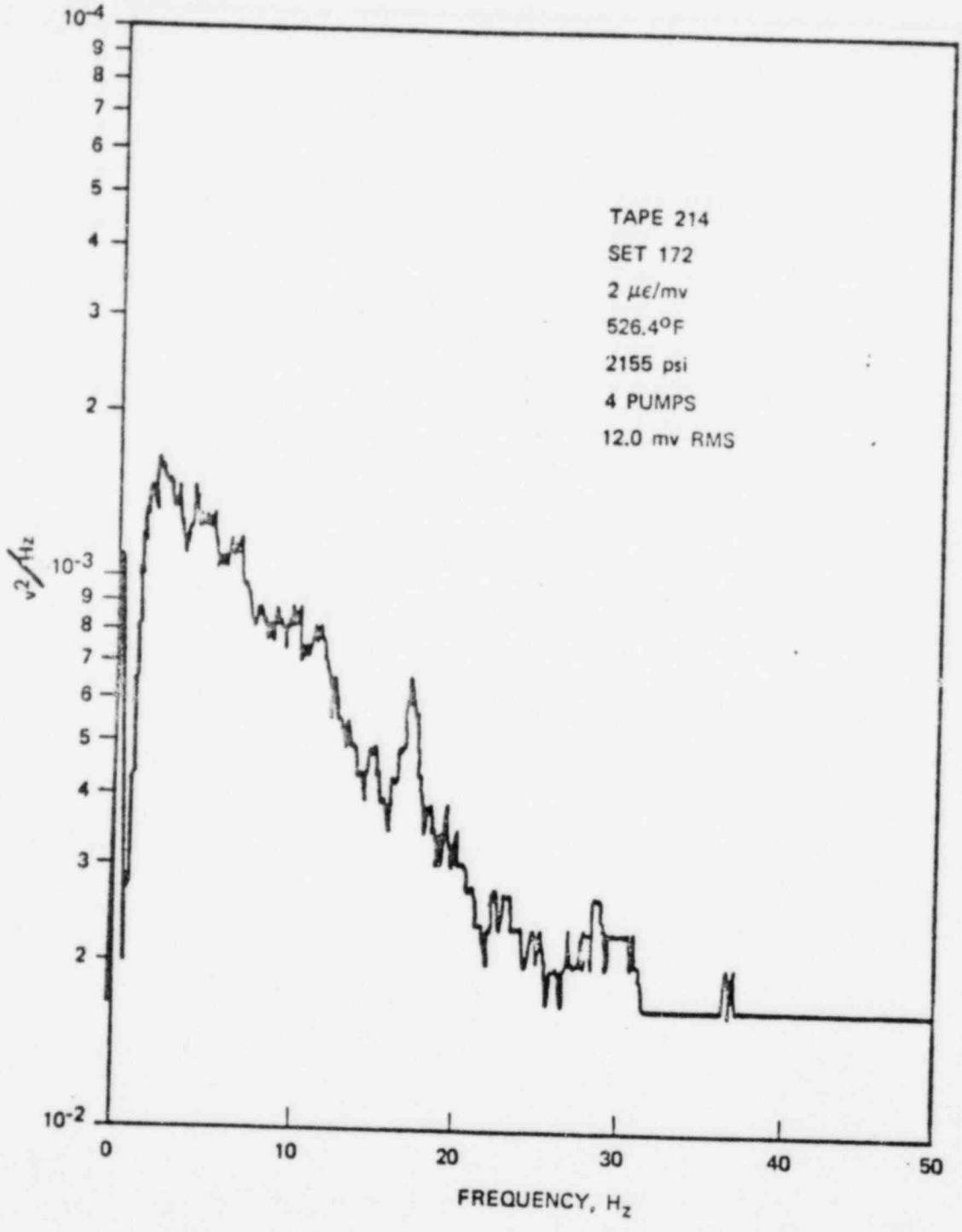

FIGURE 3.7.2 POWER SPECTRAL DENSITY, SHT2

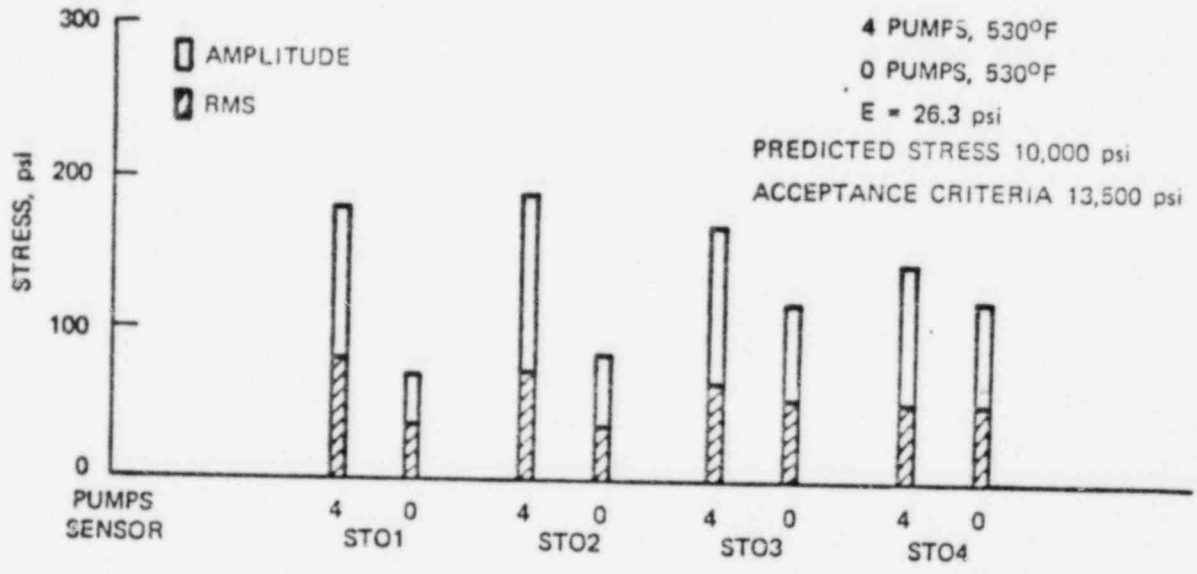

FIGURE 3.7.3 SHROUD TUBE STRESSES, RMS AND AMPLITUDE

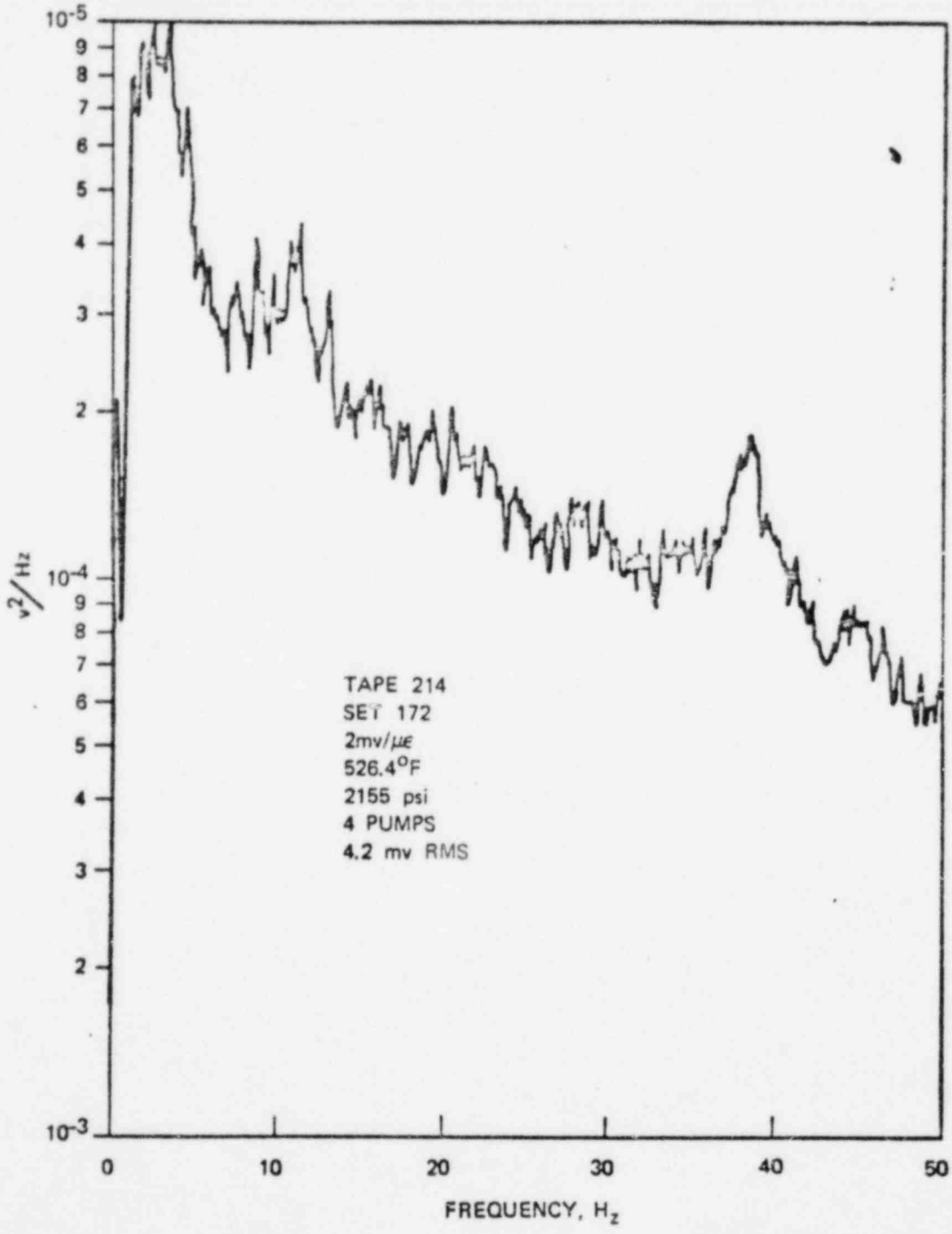

FIGURE 3.7.4 POWER SPECTRAL DENSITY, STO4

approximately 2.4 percent of the predicted stress of 10,000 psi and 1.7 percent of the acceptance criteria of 13,500 psi.

The only discernable frequency peak on the surveillance holder tube strain gages is at 17.5 Hz and on the shroud tube at 37.5 Hz. All gages show random response between 0 and 50 Hz. The frequency peaks may be caused by the thermal shield, since it is vibrating at both 17.5 Hz and 37.5 Hz.

3.8 TAPE RECORDER NOISE

3.8.1 Types of Recorded Noise

Noise seen in the playback was caused by one of three sources:

1. Sensors and conditioning equipment.

2. External noise sources; i.e., pumps, cooling fans, or other electrical equipment.

3. Electrical noise in the reproduce and record electronics.

In looking at the recorded sensor signals with no pumps operating, the magnitude of both one and three together were checked. In general, the results of the second noise source cannot be analyzed.

3.8.2 Analysis of Tape Recorder Noise

In order to determine the noise caused by the tape recorders only, the inputs to the recorders were shorted and a tape was recorded. The playback gives the noise of the record and playback recorders. In general, the only significant noise was below 10 Hz. Figure 3.8.1 shows the frequency content from recorder 2, channel 1. This is similar to most other channels. The rms value was 2.7 mv and the major frequencies were 3, 4, and 8 Hz. The frequency content of the noise is occasionally a problem when analyzing the various sensors, especially when double integration is involved. However, the total noise level is within specifications of the tape recorders.

ATTACHMENT C

SURVEILLANCE SPECIMEN HOLDER TUBE

VIBRATION DATA

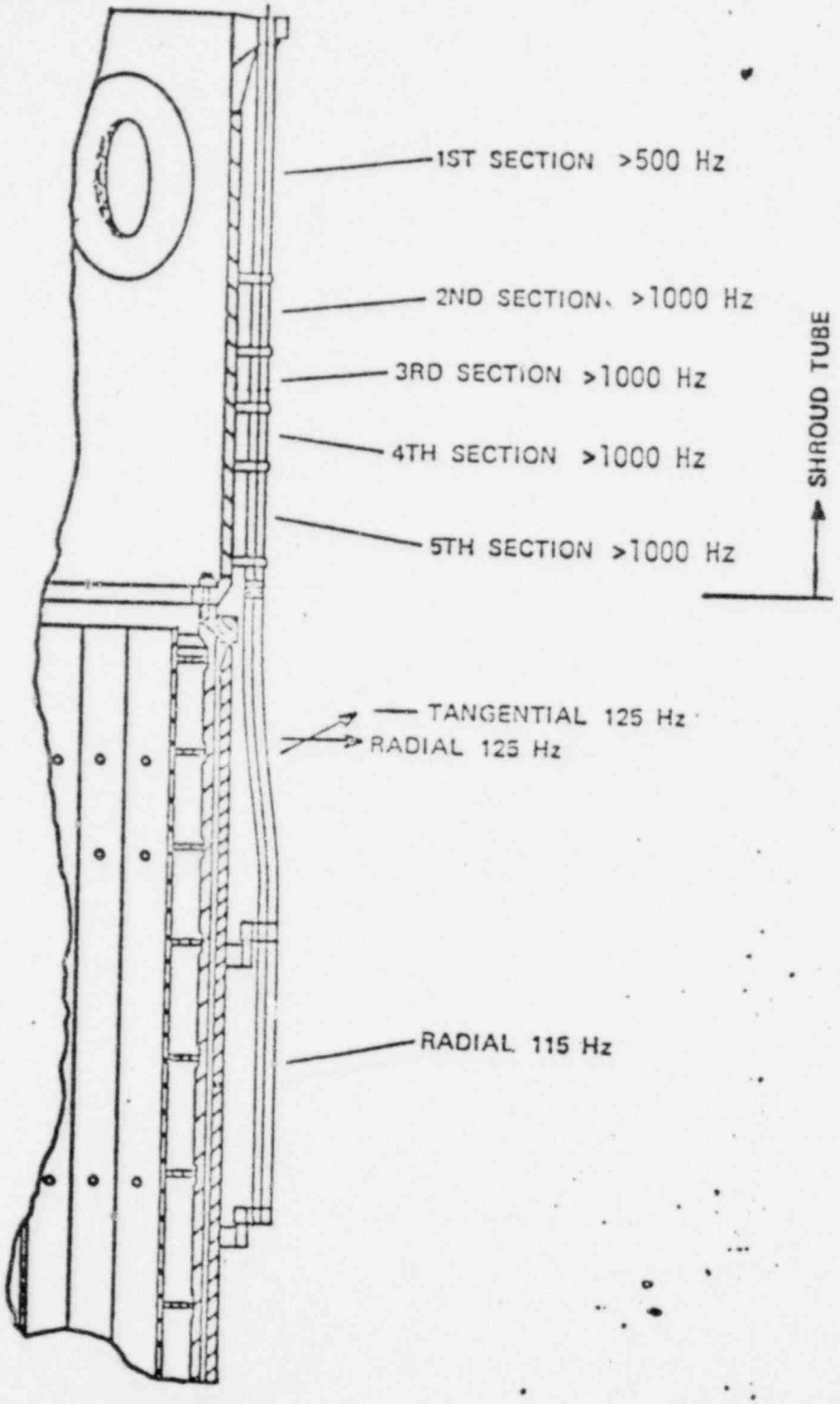

IN-AIR NATURAL FREQUENCIES

FIGURE 1

TABLE I

Component	Plant Operating Condition	Frequency-Hz	RMS Stress-psi
SSHT	4 RCP, 530°F	75 420	<500
Shroud Tube	Same	(See Note 2)	Very Low (Note 1)

NOTES:

(1) PSD's for 0 and 4 RCP are essentially the same indicating stresses are extremely low

(2) PSD's indicate broadband response to the random pressure field

INSTRUMENTATION SENSOR IDENTIFICATION
LOCATION AND ORIENTATION

Ref Dwg 34583F

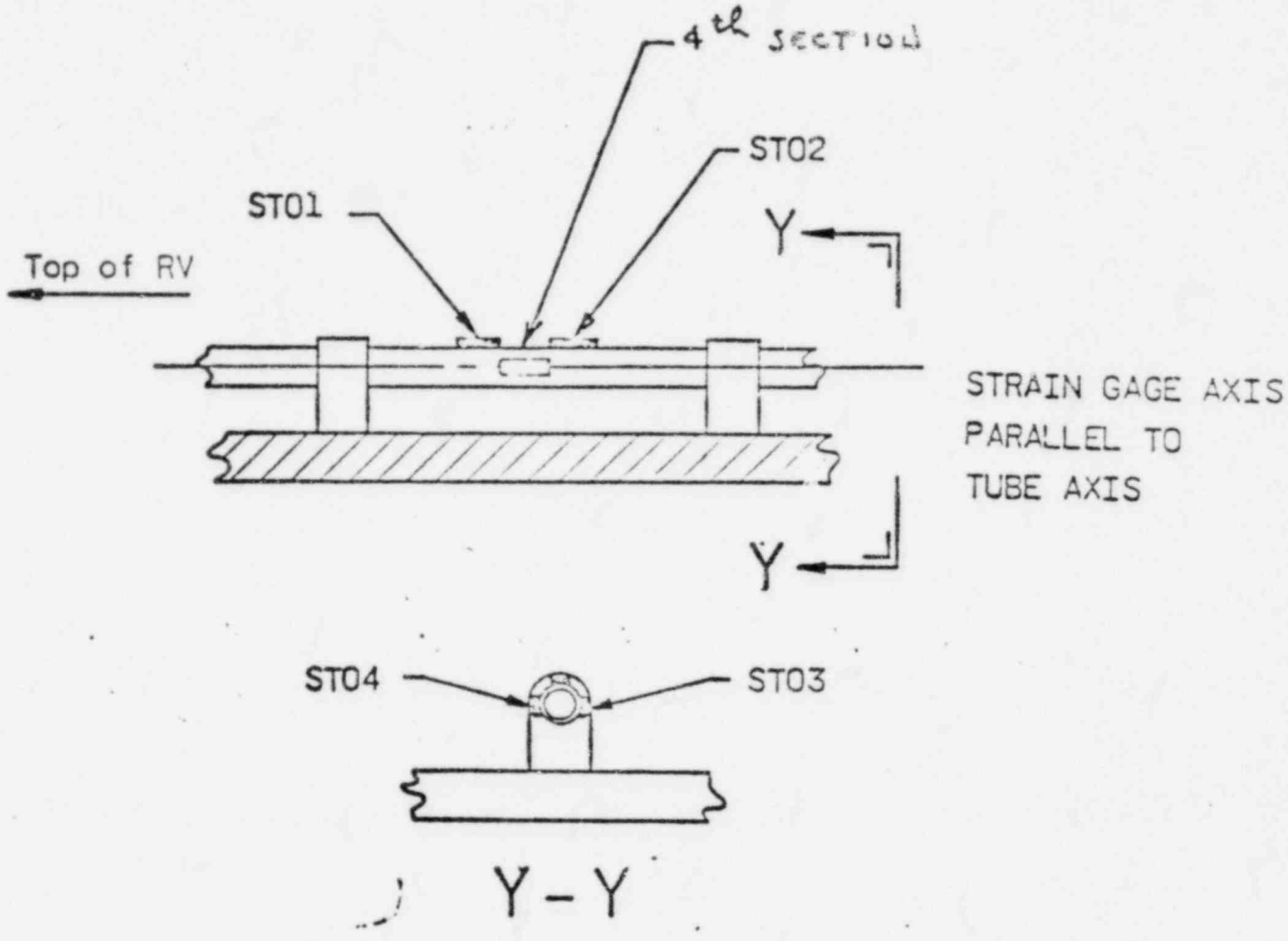

SHROUD TUBE STRAIN GAGES

ST01
ST02
ST03
ST04

FIGURE 2

INSTRUMENTATION SENSOR IDENTIFICATION
LOCATION AND ORIENTATION

Ref Dwg 34583F

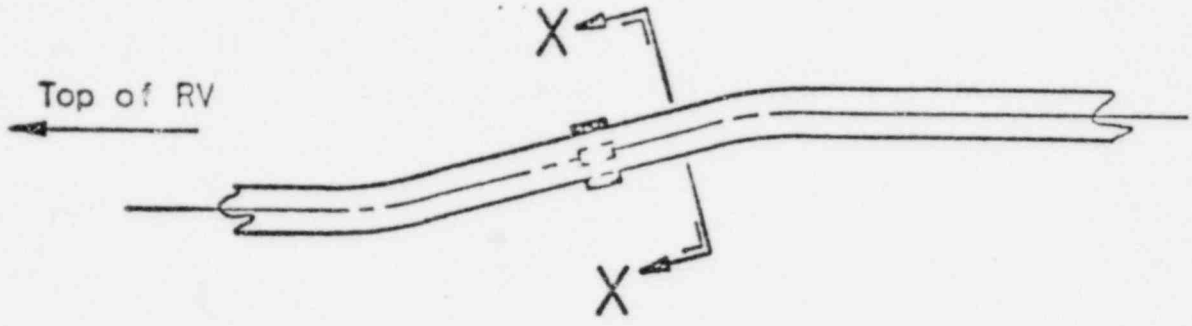

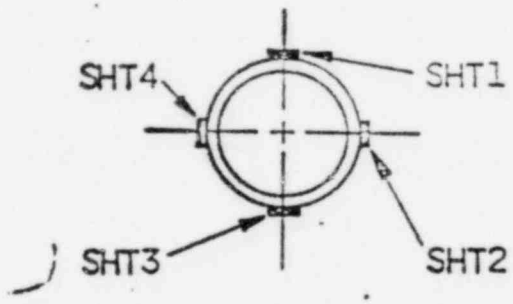

STRAIN GAGE AXIS
PARALLEL TO TUBE AXIS

X - X

SURVEILLANCE SPECIMEN HOLDER TUBE
STRAIN GAGES

SHT1
SHT2
SHT3
SHT4

FIGURE 3

ATTACHMENT D

OCONEE 1

REACTOR VESSEL SURVEILLANCE SPECIMEN

HOLDER TUBE REPORT

OCONEE 1 SURVEILLANCE SPECIMEN HOLDER TUBE REPORT

INTRODUCTION

This report provides additional information relative to the reactor vessel surveillance specimen holder tubes (SSHT) in Oconee 1. As a result of this additional information, further corrective action beyond that reported in Reference 1 is deemed necessary.

NEW INFORMATION

Duke Power Company was appraised by the Babcock & Wilcox (B&W) Company on April 5, 1976 that inspections conducted at another B&W reactor, following removal of the reactor internals, revealed evidence of wear to the SSHT journal bearing located at the bottom of the shroud tube.

CORRECTIVE ACTION

Reference 1 describes the evaluation and corrective action taken on Oconee 1 as a result of the inspections performed on the SSHT's. The inspections and evaluation did not, however, consider the new information described above. B&W advises that if excessive wear is present on the journal bearings, this has the potential for allowing excessive vibratory motion of the SSHT. Methods are available to compensate for this wear; however, they were not used on the Oconee 1 SSHT's. In order to minimize the possibility of unacceptable vibratory motion and resultant SSHT degradation occurring during cycle 3, the SSHT's and spring loaded retaining devices will be removed for the balance of cycle 3 operation.

SAFETY EVALUATION

Reactor Vessel

The request for an exemption to the requirements of 10 CFR 50, Appendix H in Reference 1 provides the justification for operation with the reactor vessel surveillance specimens removed. The additional corrective action described above does not change the evaluation or conclusions in Reference 1.

Surveillance Specimen Holder Tube

The evaluation in Reference 1 did not consider the new information described above. Should excessive wear exist on the journal bearings, the conclusion

presented that the SSHT's are structurally adequate for extended operation of Oconee 1 could be invalidated. Therefore, operation of Oconee 1 for the brief period of time until implementation of the corrective action described above has been evaluated. Due to the brevity of the period of operation, a failure is extremely unlikely to occur; however, failures in the areas of wear have been considered. Complete severance at the wear locations within the shroud tube would have no immediate effect since these portions are contained by the shroud tube. Severance at the 4th spacer location could allow this lower portion of the holder tube to oscillate on the hinged mounting brackets (pintles). This motion could be expected to wear the anti-rotation portion of the mounting bracket at the dowel pin. This wear could allow larger oscillations until eventually the upper portion of the holder tube and spring loaded retaining device could be free and could drop into the annulus between the thermal shield and the reactor vessel wall. Depending on the motion, and condition of the upper portion of the tube, it may be in one or more sections, severed at the wear locations. These sections, depending on their length, could either wedge in the annulus between the thermal shield and the reactor vessel wall, or for shorter pieces, may wedge in the lower reactor vessel head. Damage from these loose parts could occur to the reactor vessel clad, incore instrument guide tubes and the lower reactor internals. This damage would not represent an imminent threat to public health and safety, but could require extensive evaluation or repair to assure these structures remain serviceable for the life of the plant. The loose parts monitoring system at conee has proven able to detect parts much smaller than those from the failure of a holder tube and would allow an orderly shutdown should a failure occur.

CONCLUSION

It is concluded that operation of Oconee 1 for the period until implementation of the corrective action described above is acceptable. This operation and the corrective action described above will not be inimical to the health and safety of the public.

REFERENCE

1. Letter, Mr. William O. Parker, Jr., Duke Power Company, to Mr. Benard C. Rusche, NRC, RE: Oconee Unit 1, March 16, 1976.